**Advanced Journal of Chemistry, Section A**

Journal homepage: www.ajchem-a.com

Original Research Article

# An Image Analysis-Assisted Paper-Based Colorimetric Aptasensor for Simple and Rapid Malathion Detection

Mardhiahtul Iftiah Ariffin [1], Norli Abdullah [2], Nor Laili-Azua Jamari [2], Fareha Hilaluddin [2,3]*, Keat Khim Ong [2,3]*, Mohd Junaedy Osman [2], Jahwarhar Izuan Abdul Rashid [2,4], Siti Aminah Mohd Noor [2,4], Wan Md Zin Wan Yunus [1], Victor Feizal Knight [3], Chai Keong Ngan [5], Seng Teik Ten [6], Mohd Nor Faiz Norrrahim [3]

[1]*Faculty of Defence Science and Technology, Universiti Pertahanan Nasional Malaysia (National Defence University of Malaysia) (NDUM), Kuala Lumpur, Malaysia*
[2]*Department of Chemistry and Biology, Centre for Defence Foundation Studies, National Defence University of Malaysia, Kuala Lumpur, Malaysia*
[3]*Research Centre for Chemical Defence, National Defence University of Malaysia, Kuala Lumpur, Malaysia*
[4]*Centre for Tropicalisation, National Defence University of Malaysia, Kuala Lumpur, Malaysia*
[5]*Soil Science, Water & Fertiliser Research Centre, Malaysian Agricultural Research and Development Institute (MARDI), 43400 Serdang, Selangor, Malaysia*
[6]*Engineering Research Center, Malaysian Agricultural Research and Development Institute (MARDI), Selangor, Malaysia*

**ARTICLEINFO**

**Article history**

Submitted: 2025-12-02
Revised: 2025-12-30
Accepted: 2026-02-06
ID: AJCA-2512-1990
**DOI**: 10.48309/AJCA.2026.563604.1990

**KEYWORDS**

*Aptasensor*
*Image analysis*
*Paper-based colorimetric*
*Gold nanoparticles*
*Malathion*

**ABSTRACT**

Paper-based colorimetric sensors have been widely applied as cost-effective tools for on-site pesticide detection. The availability of inexpensive imaging technologies, such as smartphones, has enhanced the efficiency of detection methodologies. This work describes the development of an image analysis-assisted paper-based colorimetric aptasensor for malathion (MLT) detection. The sensing paper was fabricated by immobilizing a mixture of citrate-capped gold nanoparticles (cit-AuNPs) and thiolated DNA aptamer (Apt) onto Whatman filter paper. After a 3-minute reaction, the paper exhibited a visible color change in the presence of MLT due to cit-AuNP aggregation. Smartphone images of the sensing paper, captured before and after MLT addition, were processed using ImageJ software to obtain red, green, and blue (RGB) values, with the response expressed as ΔRGB. The aptasensor achieved a limit of detection (LOD) of 0.67 µM with a linear range of 100–1,000 µM. This paper-based colorimetric aptasensor provides a simple and rapid method for on-site MLT detection.

**GRAPHICAL ABSTRACT**

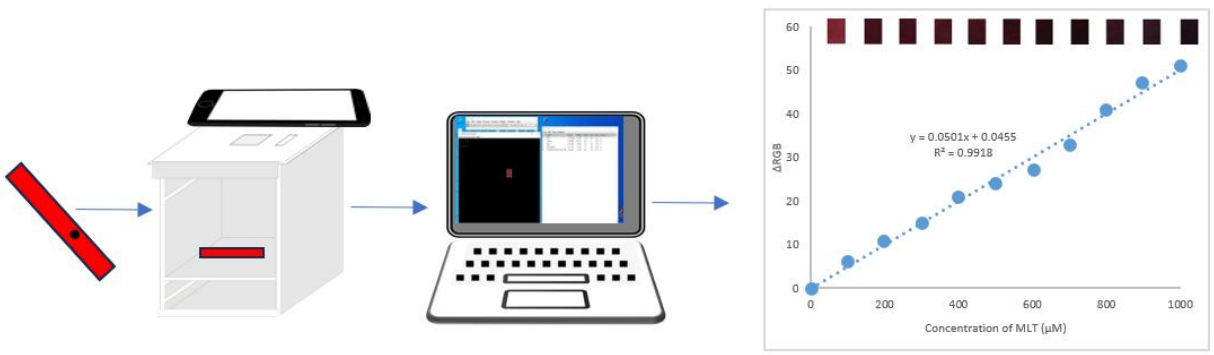


* Corresponding author: Hilaluddin, Fareha; Ong, Keat Khim
✉ E-mail: hfareha01@gmail.com; ongkhim@upnm.edu.my

## Introduction

Global farming practices largely depend on pesticides to protect crops from pests, diseases, and weeds, which can otherwise lead to a significant loss in yield and quality [1]. Based on FOA [2], the global use of pesticides in 2020 has been increased, amounting 2.7 million tonnes (Mt) of active ingredients with Asia was recorded as the most land at a high risk of pesticide pollution (1.9 million square miles) [1]. Pesticide pollution may occur through various pathways including runoff and leaching by rainfall, or spray drift during application which carried by wind, affecting non-target plants or ecosystem [3]. Among various classes of pesticides, organophosphates (OPs) are widely used not only for pest control, but also as chemical warfare agents, raising concerns about their impact on human health and the environment [4]. Due to their high toxicity and potential for exposure, OPs pose significant health risks to humans, particularly through the inhibition of acetylcholinesterase, which can lead to severe neurological and respiratory symptoms if not treated promptly [5,6]. This risk is further exacerbated by OPs contamination in food and water sources, underscoring the need for efficient detection methods to ensure food safety and environmental protection [7].

Emerging evidence suggests that organophosphate metabolites and degradation products, which may be more toxic than the parent compounds, can persist in the environment for extended periods, posing risks to non-target organisms, soil health, and water quality through runoff and leaching into aquatic ecosystems [8,9]. Despite regulatory efforts to mitigate pesticide risks, the improper use and overreliance on OPs in agriculture continue to raise concerns regarding human health, environmental sustainability, and the development of pesticide resistance in target pests [10]. As mentioned by Mostafalou & Abdollahi [11], OPs have been associated with wide range of adverse health effects on humans, including acute toxicity, neurotoxicity, developmental disorders, and increased risk of certain cancers. Therefore, accurate and efficient detection methods are essential to ensure food safety and environmental protection. Conventional detection methods for OPs typically involve complex instrumentation (*e.g.,* high performance liquid chromatography (HPLC), gas chromatography (GC), enzyme linked immunosorbent assay (ELISA)), complicated procedures, and skilled personnel that making them impractical for on-site and rapid screening applications [12,13]. Hence, there is a demand for the development of simple, cost-effective, and rapid detection techniques that can be deployed in resource-limited settings [14]. In contrast, colorimetric analysis, particularly when employed in paper-based sensors, offers a simple, rapid, and cost-effective alternative for pesticide detection [15].

Colorimetric sensors utilize specific chemical reactions between analytes and color-changing reagents, producing visible color changes that can be easily observed with the naked eye or quantified using portable devices [16]. Compared to the conventional methods, colorimetric analysis eliminates the need for sophisticated equipment and extensive sample preparation, making it suitable for on-site and field applications [17]. Additionally, colorimetric sensors can be designed for multiplex detection of multiple analytes simultaneously, further enhancing their utility for screening purposes [18]. Despite their simplicity, colorimetric sensors demonstrate competitive sensitivity and selectivity, offering a promising approach for rapid and accessible detection of pesticide contamination in various matrices [19].

Paper-based analytical devices (PADs) have been increasingly employed for environmental monitoring, including the detection of pesticide residues in water sources, soil, and air,

highlighting their versatility and relevance in addressing environmental challenges [20]. In recent years, PADs have gained significant attention as promising platforms for pesticide detection due to their simplicity, portability, low cost, and ease of fabrication [21,22]. Recent studies have shown significant advancements of PADs, particularly in terms of sensitivity, selectivity, and fabrication techniques [23]. Incorporating nanomaterials such as gold nanoparticles (AuNPs) and carbon nanotubes into PADs has been shown to enhance their detection capabilities for various analytes, including pesticides [24]. Coupled with colorimetric detection strategies, these sensors offer a convenient means for visualizing analyte concentrations without the need for specialized equipment, as they provide a visible and easily interpretable response [25,26].

Detecting pesticides in water using smartphone platforms offers a promising avenue for rapid and accessible environmental monitoring [27]. Leveraging the computational capabilities and connectivity of smartphones, innovative aptasensor technologies can be integrated to enable real-time detection and analysis of pesticide residues in water samples [28]. Recently, the integration of smartphones in detecting pesticides residues in environmental samples has earned significant research attention [29–31]. By coupling paper-based colorimetric aptasensor or other portable detection platforms with smartphone applications, users can easily capture images of the colorimetric response and receive instant feedback on pesticide concentrations [32]. According to Ateia *et al*. [33], this approach not only enhances the efficiency and convenience of pesticide monitoring, but also empowers communities, researchers, and regulatory agencies to monitor water quality more effectively and respond promptly to potential contamination events. Furthermore, the widespread availability of smartphones ensures that this technology can be deployed across diverse geographical locations, facilitating comprehensive monitoring efforts and contributing to the protection of water resources and public health. In this study, paper-based colorimetric aptasensor for rapid detection of MLT was developed. A commercial laboratory filter paper (Whatman filter paper Grade 1) was modified with deposition of cit-AuNPs and Apt. The colour of the modified filter papers before and after detection with MLT were captured in an image capturing box using a smartphone at a fixed distance between the modified filter paper and the smartphone. The image capturing box was designed using three-dimensional (3D) printer to enable fast prototyping. The captured images were easily interpreted using ImageJ. By combining the simplicity and portability of paper-based aptasensors with the smartphones, this study aimed to develop a robust sensing platform capable of detecting MLT at micromolar (100-1000 µM) levels, thereby enabling timely intervention and mitigation of pesticide contamination in food and water resources.

## Experimental

### *Materials and reagents*

The chemicals used in this study are gold (III) chloride trihydrate ($HAuCl_4 \cdot 3H_2O$), MLT ($C_{10}H_9O_6PS_2$) and acetonitrile ($CH_3CN$), which were purchased from Sigma-Aldrich (USA), whereas trisodium citrate dihydrate ($C_6H_5Na_3O_7 \cdot 2H_2O$) was obtained from Merck (German). The Whatman® qualitative filter paper (Grade 1) with thickness of 180 µm and diameter of 90 mm was obtained from Cytiva (Marlborough, USA). The IDTE solution and thiol-modified DNA aptamer (Apt) used in this study was provided by integrated DNA Technologies (Singapore) with a sequence of 5' -ThioMC6D-ATC CGT CAC ACC TGC TCT TAT ACA CAA TTG TTT TTC TCT TAA CTT CTT GAC TGC TGG TGT TGG CTC CCG TAT-3'. The sequence of the thiolated

DNA aptamer was prepared according to Abnous *et al*. [34].

*Synthesis of citrate capped AuNPs (cit-AuNPs)*

In this study, synthesis of citrate capped AuNPs (cit-AuNPs) was conducted as reported by Ariffin *et al*. [35]. 250 mL of 1.5 mM of $HAuCl_4 \cdot 3H_2O$ was initially stirred (1,000 rpm) and heated until boil at 100 °C, followed by rapid addition of 25 mL of 38.8 mM of trisodium citrate solution. The reaction mixture was continuously stirred and heated until the yellowish gold (Au) solution turns red. The suspension was then cooled to room temperature and stored in an amber glass bottle at 4 °C for further use.

*Fabrication of paper-based colorimetric aptasensor*

A paper-based colorimetric aptasensor was prepared using a clean Whatman filter paper (WFP). The filter paper was cut into rectangular shape (size: 0.5 cm (width) x 3.0 cm (length)) and rinsed with milli-Q water before dried in an oven at 50 °C for 40 mins. Then, 10 rectangular filter papers were directly soaked in 20 mL of ethanol in a petri dish (diameter: 14 cm) for 1 hour. The rectangular filter papers were rinsed 2 times with Milli-Q water and left to dry at room temperature for 1.5 hours. Subsequently, the dried filter papers were immersed in a mixture (consists of 990 µL of cit-AuNPs and 10 µL of DNA aptamer (3 nM)) for 1 hour, and then rinsed with Milli-Q water. Afterward, the modified filter paper (WFP-AuNPs-Apt) was rinsed with Milli-Q water and left to dry at room temperature for 10 mins before used for detection. The fabrication steps of WFP-AuNPs-Apt conducted in this study is displayed in Figure 1.

*Characterisation of cit-AuNPs*

*Ultraviolet-Visible (UV-Vis) Spectroscopy*

An UV-Vis spectrophotometer (UV-3600i plus, Shimadzu, Japan) was used for characterization of cit-AuNPs. The synthesized cit-AuNPs was diluted with Mili-Q water and then placed in a quartz cuvette. The absorbance was measured from 400 nm to 800 nm. The stability of the cit-AuNPs was also examined by measuring the UV-Vis absorbance of cit-AuNPs for a period of 49 days.

*High resolution transmission electron microscopy (HRTEM)*

The shape and particle size of synthesized cit-AuNPs were characterised using HRTEM (JEOL, JEM-2100F, Japan). The synthesized cit-AuNPs (10 µL) was deposited on top of the copper (Cu) grid and air dried for 4 hours at room temperature before the analysis was performed at an acceleration voltage of 160 kV. The particle size distribution of the cit-AuNPs was evaluated through a random sampling of 200 individual particles from the TEM images to ensure statistical accuracy.

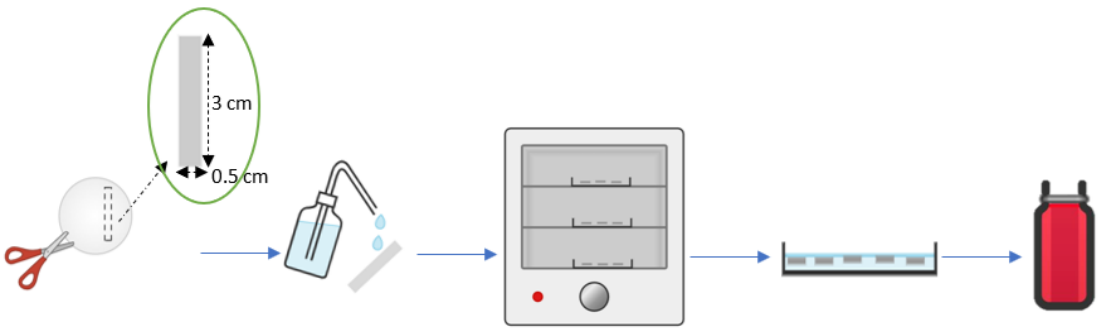


**Figure 1**. Fabrication steps of the WFP-AuNPs-Apt proposed in this study

*Preparation of MLT stock and working solutions*

To prepare 100 mL of 2.5 mM of MLT stock solution, a desired amount of MLT was added into a mixture of acetonitrile and MiliQ water (volume ratio: 1:1). Different concentrations (100, 200, 300, 400, 500, 600, 700, 800, 900, and 1,000 µM) of MLT solutions were then prepared from MLT stock solution to develop a calibration curve for MLT detection.

*Calibration curve for MLT detection*

To construct a calibration curve, the fabricated WFP-AuNPs-Apt aptasensor was evaluated for MLT detection using different concentrations of MLT (100 to 1,000 µM). Each detection experiment was conducted in triplicates at room temperature, and a similar experimental procedure was applied for the blank. A smartphone (iPhone 7) was used to acquire digital images of the solutions with the aid of a 3D-printed image capturing box. The schematic diagram for the quantitative determination of MLT using the WFP-AuNPs-Apt sensor assisted with image analysis is illustrated in Figure 2. At first, 7 µL of MLT was dropped onto a point on the WFP-AuNPs-Apt sensor located 0.5 cm from the bottom margin and 0.25 cm from the left margin. After dropping with MLT, the WFP-AuNPs-Apt sensor was then placed in the 3D-printed image-capturing box. The dimensions of the 3D-printed image capturing box are shown in Figure 3. The aptasensor was captured using a smartphone under constant conditions after a detection period of 3 minutes, at a fixed distance of 7.5 cm between the smartphone and the WFP-AuNPs-Apt sensor. Afterward, the images were imported into a laptop and analysed using ImageJ software to quantify colour intensity in terms of red, green, and blue (RGB) values. A fixed rectangular region of interest (ROI) was selected in each image using the selection tool of the software to ensure consistency across samples. The RGB values within the selected area were then measured using the software, and the resulting data were displayed on the screen. These RGB values were subsequently exported and further processed in Microsoft Excel, where response (ΔRGB) values were calculated based on the equation reported by Murdock *et al.* [36]. Eventually, a calibration curve for MLT detection was constructed to establish the relationship between ΔRGB and MLT concentration.

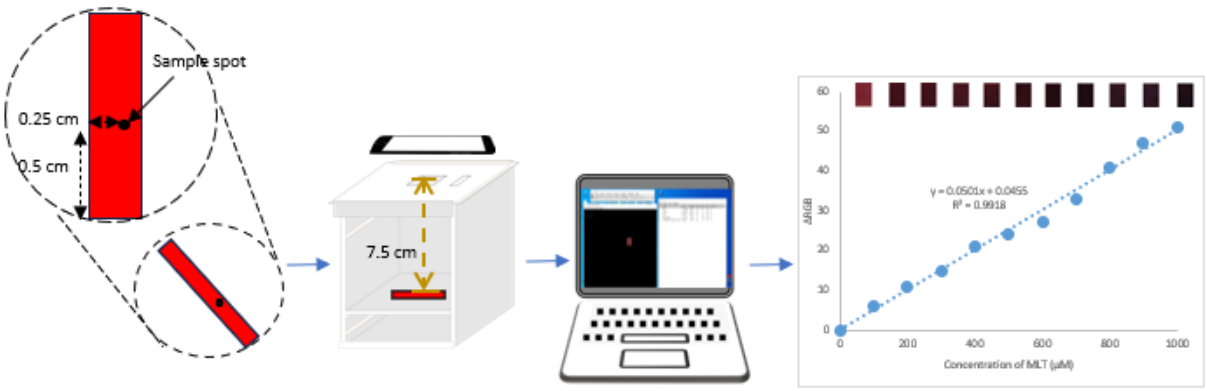


**Figure 2.** Schematic illustration of MLT detection using WFP-AuNPs-Apt aptasensor incorporated with image analysis

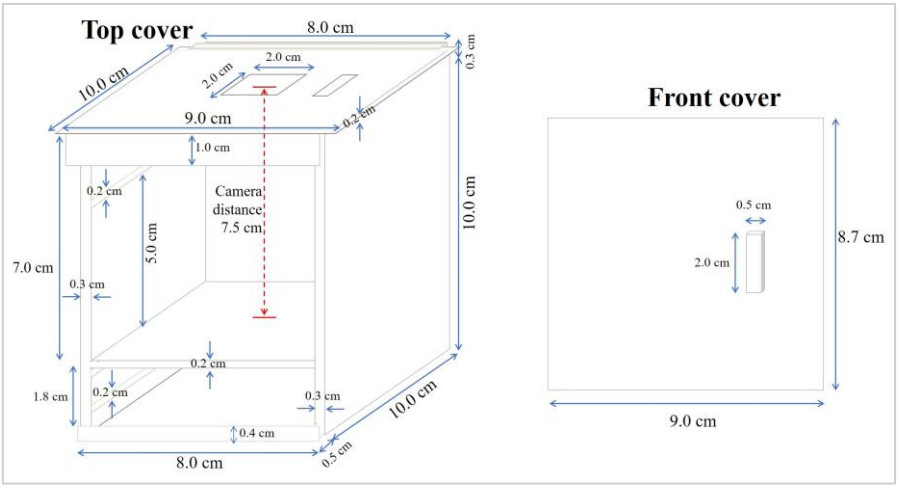


**Figure 3.** Dimensions of 3D-printed image capturing box used in this study

*Image analysis*

The captured WFP-AuNPs-Apt aptasensor images were imported into a laptop and analysed using ImageJ software to quantify colour intensity in terms of red, green, and blue (RGB) values. A fixed rectangular ROI was selected in each image using the software's selection tool (Figure 4a) to ensure consistency across samples. The undesired areas adjacent to this region were omitted using the *Edit → Clear Outside* function (Figure 4b). Thereafter, the RGB values were within the selected area were extracted via *Plugins → Analyze → RGB Measure* (Figure 4c), and the resulting values were displayed on the screen as illustrated in Figure 4d. These RGB values were subsequently exported and further processed in Microsoft Excel, where response (ΔRGB) values were calculated based on the equation reported by Murdock *et al*. [36].

## Results and Discussion

*Characterisation of cit-AuNPs*

*UV-Vis spectroscopy*

The successful synthesis of cit-AuNPs was confirmed by their distinct bright red color by UV-Vis spectroscopy analysis. This technique is highly effective for characterizing various metal nanoparticles formation because examination of the localized surface plasmon resonance (SPR) band offers indirect the evidence which supporting the AuNPs formation as reported by a previous work [37]. Based on the UV-Vis spectrum of cit-AuNPs, as illustrated in Figure 5, a localized SPR peak observed at $\lambda_{max}$ of 521 nm, indicating the presence of spherical AuNPs, which consistent with the characterization of 20 nm AuNPs reported by a previous study [38]. In addition, Sangwan and Seth [39] reported that the desirable optical properties of successful synthesis of AuNPs are within range of 520-525 nm.

*High resolution transmission electron microscopy (HRTEM)*

Based on the TEM image of cit-AuNPs in Figure 6a, the cit-AuNPs exhibited a predominantly spherical shape and well dispersed in the solution. The histogram (Figure 6b) shows a relatively narrow distribution, with an average particle size of 13 ± 0.58 nm. The narrow and well-defined peak of particle size distribution show a relatively uniform size distribution of NPs that well-dispersed (monodisperse), with minimal aggregation and relatively small in size [40].

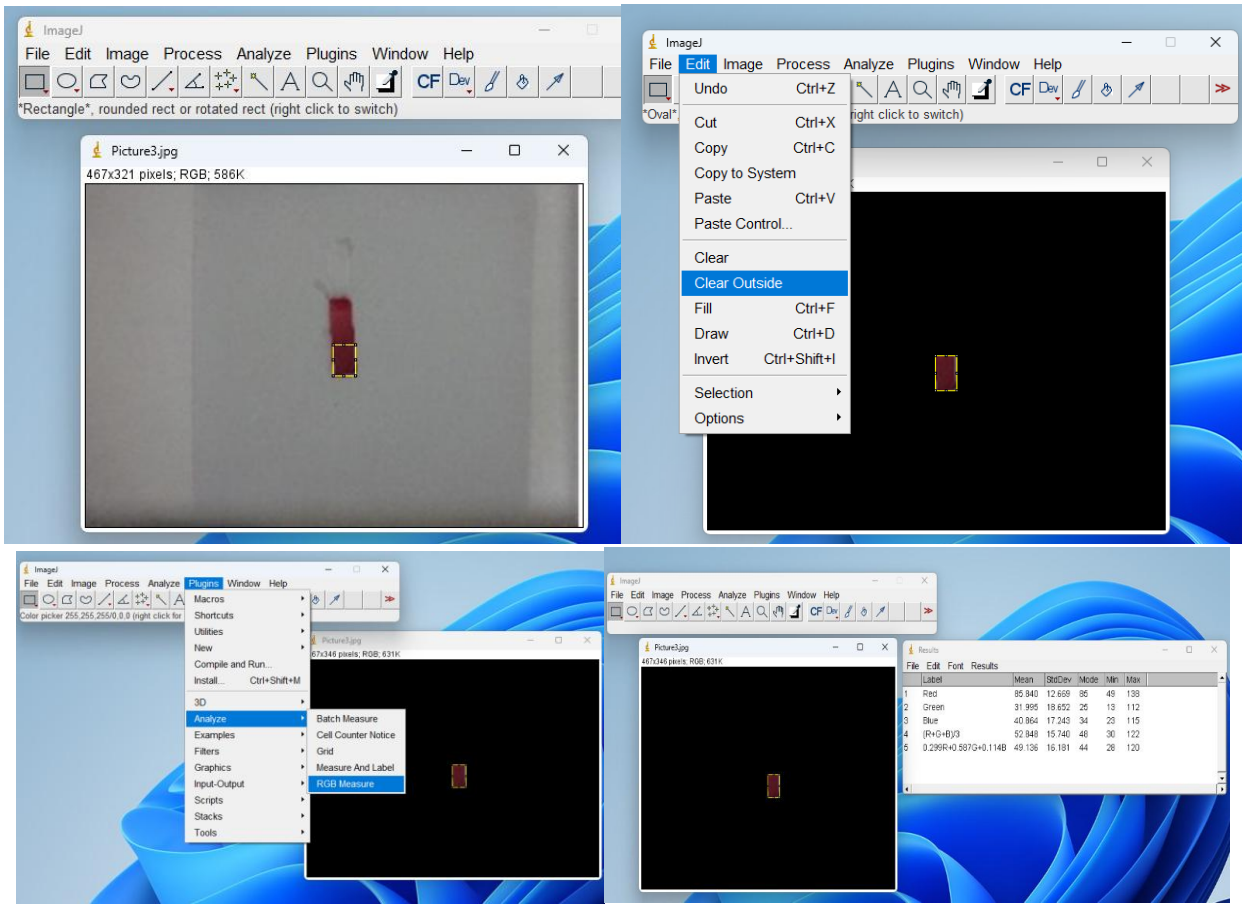


**Figure 4.** The captured images are analysed using ImageJ software by following these steps: (a) the 'rectangular' tool is selected to highlight the desired area with a rectangular shape, (b) the undesirable area of the captured image is cleared by clicking *Edit* → *Clear Outside*, (c) the RGB values of the cropped image are measured by clicking *Plugins* → *Analyze* → *RGB Measure*, and (d) the RGB values are displayed on the screen.

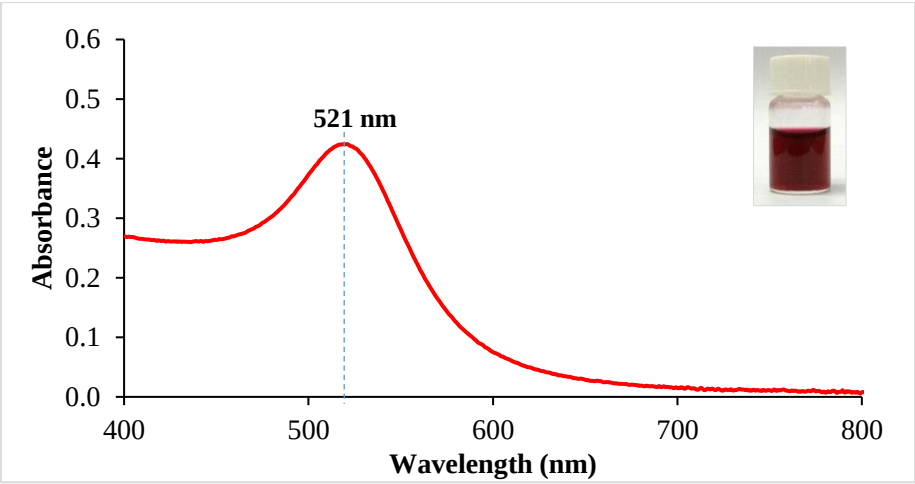


**Figure 5.** UV-Vis spectrum of cit-AuNPs. Inset: image of synthesised cit-AuNPs

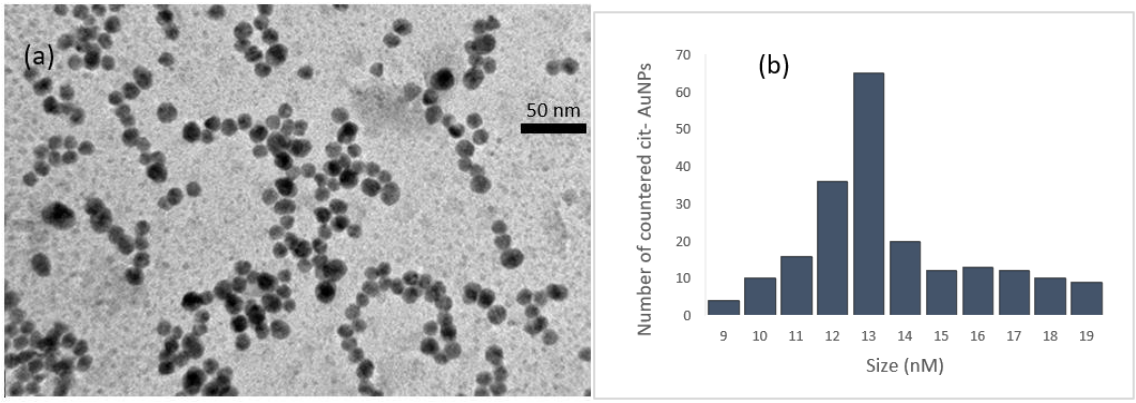


**Figure 6.** Particle characterisation of cit-AuNPs solution (a) TEM image of cit-AuNPs, with a scale bar of 50 nm, and (b) histogram of cit-AuNPs particle size distribution

*Stability of cit-AuNPs*

The stability of the cit-AuNP colloidal suspension was evaluated by monitoring changes in UV–Vis absorbance over 49 days using the UV–Vis spectrophotometer. The UV–Vis spectra corresponding to these periods are shown in Figure 7. During this period, the $\lambda_{max}$ remained constant at around 521 nm, which is the characteristic SPR peak of cit-AuNPs. According to Park *et al*. [41], the negatively charged citrate ions adsorb onto the AuNPs surface, imparting a negative charge layer that generates electrostatic repulsion between particles. This repulsion counteracts the attractive van der Waals forces, preventing aggregation and helping maintain a uniform distribution of charge, which stabilise the cit-AuNPs. Further analysis of these results was performed using a paired *t*-test, and the findings are presented in Table 1.

Table 1 shows the results of a paired t-test analysis of the mean absorbance of cit-AuNPs measured at $\lambda_{max}$ over 49 days. The t-test results (Table 1) were used to statistically compare the absorbance values measured at $\lambda_{max}$ on day 1 with those collected on subsequent days (day 3 through day 30). The standard deviations (SDs) of the mean absorbance values are low (0.0008 to 0.0684) over time, suggesting minimal experimental variation that was not sufficient to affect the overall statistical significance. The obtained *p*-values were 0.2793 and 0.3149 for days 3 and 7, respectively, both of which were greater than 0.05. This indicates that there was no statistically significant difference in absorbance between days 1 and 3, as well as between days 1 and 7. However, most of the *p*-values less than 0.05 were observed from day 10 until day 49, indicating that the absorbance measured at $\lambda_{max}$ changed significantly beginning on day 10. This minor reduction in absorbance intensity may indicate a small degree of sedimentation or optical dilution over time. However, the unchanged $\lambda_{max}$ confirms that the nanoparticles did not undergo significant aggregation or shape transformation. No evidence of aggregation, peak broadening, or red-shifting of the SPR peak was observed, suggesting that the cit-AuNPs remained physically and chemically stable under the given storage conditions for 7 days.

*Mechanism of MLT detection using cit-AuNPs-Apt*

The schematic diagram of MLT detection mechanism using the cit-AuNPs-Apt proposed in this study is shown in Figure 8a. Upon Apt addition to cit-AuNPs, the Apt replaced the citrate ligands on the surface of monodispersed AuNPs via physical adsorption due to stronger Au-S bond that displaces the weakly citrate bond, and makes the AuNPs more stable [42].

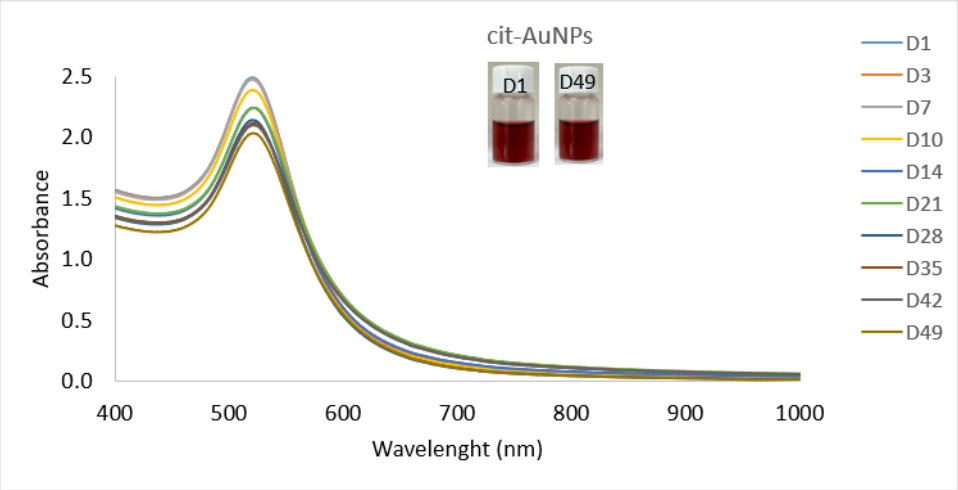


**Figure 7.** Variation in UV-Vis absorbance of cit-AuNPs from day 1 to day 49

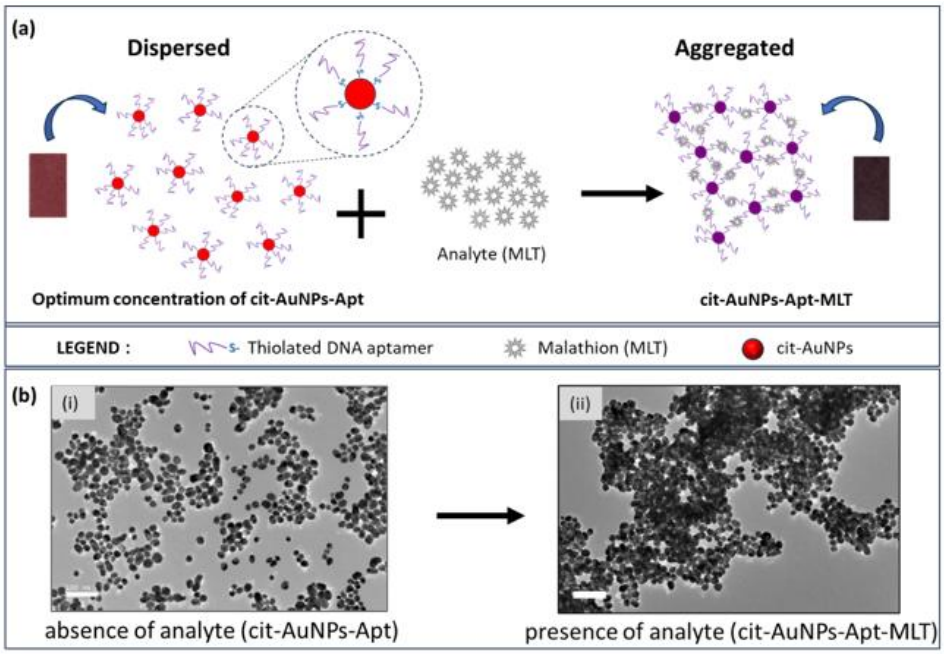


**Figure 8.** (a) Schematic illustration of MLT detection mechanism using a WFP-AuNPs-Apt sensor; (b) TEM images: (i) cit-AuNPs-Apt remain dispersed in the absence of MLT, and (ii) cit-AuNPs-Apt aggregate in the presence of MLT (scale bar: 100 nm)

**Table 1.** Independent *t*-test results of mean absorbance of cit-AuNPs at $\lambda_{max}$

| Day | 1 | 3 | 7 | 10 | 14 | 21 | 28 | 35 | 42 | 49 |
|---|---|---|---|---|---|---|---|---|---|---|
| **Mean absorbance** | 2.5073 | 2.4869 | 2.4812 | 2.4027 | 2.2702 | 2.2663 | 2.1606 | 2.0700 | 2.0609 | 2.0105 |
| **SD** | 0.0190 | 0.0055 | 0.0008 | 0.0154 | 0.0321 | 0.0310 | 0.0214 | 0.0684 | 0.0639 | 0.0385 |
| ***P*- value** | - | 0.2793 | 0.3149 | 0.0155 | 0.0248 | 0.0223 | 0.0031 | 0.0507 | 0.0451 | 0.0176 |

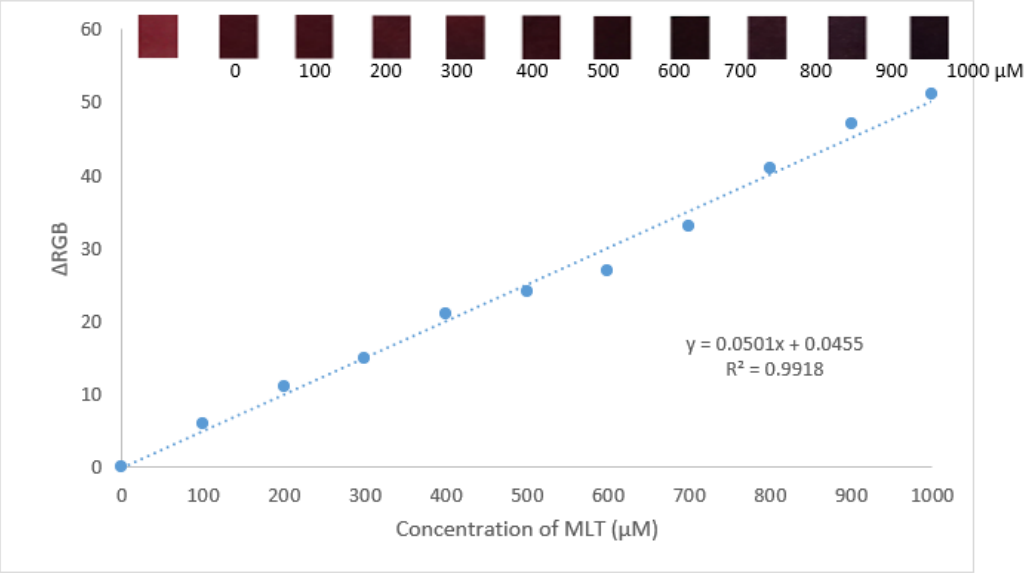


**Figure 9.** Calibration curve for MLT detection using WFP-AuNPs-Apt sensor, showing the correlation between MLT concentration and the corresponding colorimetric change (ΔRGB). The images above the graph represent the visual color changes associated with varying MLT concentrations, illustrating the sensor's response.

In the presence of an analyte (MLT), the aptamer changes its conformation from a random coil to a rigid structure due to its strong affinity for the analyte, and dissociates from the AuNPs to bind with the analyte, resulting in the AuNPs aggregation [43,44]. This aggregation caused color change of cit-AuNPs from red to deep reddish-purple. The aggregation of cit-AuNPs-Apt after MLT detection was further confirmed by TEM images (Figure 8b). The TEM image shows that the cit-AuNPs-Apt remain dispersed in the absence of MLT (Figure 8b (i)), while aggregated upon MLT addition (Figure 8b (ii)), forming cit-AuNPs-Apt-MLT complexes.

*Calibration curve*

The fabricated WFP-cit-AuNPs-Apt sensor was applied for the quantitative analysis of MLT in the range of 100 to 1,000 µM. A visible color change in the WFP-cit-AuNPs-Apt sensor was observed upon the MLT addition. A calibration curve for the MLT detection was generated by plotting ΔRGB values against MLT concentrations (Figure 9). A good linear relationship (y = 0.0501x + 0.0455, where *y* is the mean ΔRGB value and *x* is the MLT concentration) was obtained over the range of 100 to 1,000 µM of MLT, with a correlation coefficient of $R^2$ = 0.9918, indicating a strong correlation between ΔRGB and MLT concentration. The limit of detection (LOD) was calculated to be 0.67 µM based on the equation described by Feng *et al*. [45].

## Conclusion

A colorimetric aptasensor using cit-AuNPs-Apt as a sensing reagent was successfully employed for the detection of MLT. The aptasensor enabled quantitative detection of MLT using a smartphone within 3 minutes. Integration of the aptasensor with image analysis proved to be a valuable approach for MLT quantification. Under optimal conditions, the developed paper-based aptasensor demonstrated a linear detection range of 100 to 1,000 µM, with a LOD of 0.67 µM. In conclusion, a promising paper-based aptasensor for the simple and rapid quantitative detection of MLT was successfully developed. However, further research is needed to assess selectivity

and perform real sample analysis to validate the practical applicability and reliability of this aptasensor for on-site detection.

## Acknowledgements

The present work was funded through (UPNM/2018/CHEMDEF/ST/2) from Ministry of Higher Education Malaysia and (PS078-UPNM/2023/GPPP/ST/4) from National Defence University of Malaysia (NDUM) for postdoctoral fellowship. The authors would also like to gratefully acknowledge UPNM for providing the facilities for the research.

## Disclosure Statement

No potential conflict of interest was reported by the authors.

## ORCID

*Norli Abdullah:*
*https://orcid.org/0000-0002-8519-3379*
*Nor Laili-Azua Jamari:*
*https://orcid.org/0000-0002-5343-7906*
*Fareha Hilaluddin:*
*https://orcid.org/0000-0001-6128-8990*
*Keat Khim Ong:*
*https://orcid.org/0000-0002-6549-6540*
*Mohd Junaedy Osman:*
*https://orcid.org/0000-0002-3230-0505*
*Jahwarhar Izuan Abdul Rashid:*
*https://orcid.org/0000-0002-2071-4954*
*Wan Md Zin Wan Yunus:*
*https://orcid.org/0000-0003-0057-3784*
*Victor Feizal Knight:*
*https://orcid.org/0000-0003-0060-4931*
*Chai Keong Ngan:*
*https://orcid.org/0009-0006-1082-008X*
*Mohd Nor Faiz Norrrahim:*
*https://orcid.org/0000-0003-2101-5642*

## References

[1] Raj, A., Dubey, A., Malla, M.A., Kumar, A. Pesticide pestilence: Global scenario and recent advances in detection and degradation methods. *J. Environ. Manage.*, **2023,** *338*, 117680.
[2] Wanner, N., DeSantis, G., Alcibiade, A., Tubiello, F.N. Pesticides Use, Pesticides Trade and Pesticides Indicators: Global, Regional and Country Trends, 1990–2020; FAOSTAT Analytical Brief 46, FAO Food and Nutrition Series; FAO: Rome, Italy, **2022**.
[3] Hewitt, A.J. Adjuvant use for the management of pesticide drift, leaching and runoff. *Pest Management Science*, **2024**, 80(10), 4819-4827.
[4] Lu, X., Zhang, Z., Gao, R., Wang, H., Xiao, J. Recent progress in the chemical attribution of chemical warfare agents and highly toxic organophosphorus pesticides. *Forensic Toxicology*, **2021**, 39(2), 334-349.
[5] Aroniadou-Anderjaska, V., Figueiredo, T.H., de Araujo Furtado, M., Pidoplichko, V.I., Braga, M.F. Mechanisms of organophosphate toxicity and the role of acetylcholinesterase inhibition. *Toxics*, **2023**, 11(10), 866.
[6] Čadež, T., Kolić, D., Šinko, G., Kovarik, Z. Assessment of four organophosphorus pesticides as inhibitors of human acetylcholinesterase and butyrylcholinesterase. *Scientific Reports*, **2021**, 11(1), 21486.
[7] Leskovac, A., Petrović, S., Pesticide use and degradation strategies: Food safety, challenges and perspectives. *Foods*, **2023**, 12(14), 2709.
[8] Sánchez-Bayo, F., Hyne, R.V. Detection and analysis of neonicotinoids in river waters–development of a passive sampler for three commonly used insecticides. *Chemosphere*, **2014**, 99, 143-151.
[9] van den Berg, H., Gu, B., Grenier, B., Kohlschmid, E., Al-Eryani, S., da Silva Bezerra, H.S., Nagpal, B.N., Chanda, E., Gasimov, E., Velayudhan, R. Pesticide lifecycle management in agriculture and public health: Where are the gaps? *Science of the Total Environment*, **2020**, 742, 140598.
[10] Boedeker, W., Watts, M., Clausing, P., Marquez, E. Retracted article: The global distribution of acute unintentional pesticide poisoning: Estimations based on a systematic review. *BMC Public Health*, **2020**, 20(1), 1875.
[11] Mostafalou, S., Abdollahi, M. Pesticides: An update of human exposure and toxicity. *Archives of Toxicology*, **2017**, 91(2), 549-599.
[12] Brinco, J., Guedes, P., da Silva, M.G., Mateus, E.P., Ribeiro, A.B. Analysis of pesticide residues in soil: A review and comparison of methodologies. *Microchemical Journal*, **2023**, 195, 109465.

[13] Yao, J., Wang, Z., Guo, L., Xu, X., Liu, L., Xu, L., Song, S., Xu, C., Kuang, H. Advances in immunoassays for organophosphorus and pyrethroid pesticides. *TrAC Trends in Analytical Chemistry*, **2020**, 131, 116022.
[14] Xu, L., Abd El-Aty, A., Eun, J.-B., Shim, J.-H., Zhao, J., Lei, X., Gao, S., She, Y., Jin, F., Wang, J. Recent advances in rapid detection techniques for pesticide residue: A review. *Journal of Agricultural and Food Chemistry*, **2022**, 70(41), 13093-13117.
[15] Fuyal, M., Giri, B. A combined system of paper device and portable spectrometer for the detection of pesticide residues. *Food Analytical Methods*, **2020**, 13(7), 1492-1502.
[16] Kumar, V., Vaid, K., Bansal, S.A., Kim, K.H. Nanomaterial-based immunosensors for ultrasensitive detection of pesticides/herbicides: Current status and perspectives. *Biosensors and Bioelectronics*, **2020**, 165, 112382.
[17] Umapathi, R., Sonwal, S., Lee, M.J., Rani, G.M., Lee, E.-S., Jeon, T.-J., Kang, S.-M., Oh, M.-H., Huh, Y.S. Colorimetric based on-site sensing strategies for the rapid detection of pesticides in agricultural foods: New horizons, perspectives, and challenges. *Coordination Chemistry Reviews*, **2021**, 446, 214061.
[18] Huang, J., Zhu, X.-L., Wang, Y.-M., Ge, J.-H., Liu, J.-W., Jiang, J.-H. A multiplex paper-based nanobiocatalytic system for simultaneous determination of glucose and uric acid in whole blood. *Analyst*, **2018**, 143(18), 4422-4428.
[19] Issaka, E., Wariboko, M.A., Johnson, N.A.N., Nyame-do Aniagyei, O. Advanced visual sensing techniques for on-site detection of pesticide residue in water environments. *Heliyon*, **2023**, 9(3).
[20] Chen, H., Zhang, L., Hu, Y., Zhou, C., Lan, W., Fu, H., She, Y. Nanomaterials as optical sensors for application in rapid detection of food contaminants, quality and authenticity. *Sensors and Actuators B: Chemical*, **2021**, 329, 129135.
[21] Ozer, T., McMahon, C., Henry, C.S. Advances in paper-based analytical devices. *Annual Review of Analytical Chemistry*, **2020**, 13(1), 85-109.
[22] Bordbar, M.M., Sheini, A., Hashemi, P., Hajian, A., Bagheri, H. Disposable paper-based biosensors for the point-of-care detection of hazardous contaminations—a review. *Biosensors*, **2021**, 11(9), 316.
[23] Martínez-Pérez-Cejuela, H., Mesquita, R.B., Simó-Alfonso, E., Herrero-Martínez, J., Rangel, A.O. Combining microfluidic paper-based platform and metal–organic frameworks in a single device for phenolic content assessment in fruits. *Microchimica Acta*, **2023**, 190(4), 126.
[24] Li, Z., Lin, H., Wang, L., Cao, L., Sui, J., Wang, K. Optical sensing techniques for rapid detection of agrochemicals: Strategies, challenges, and perspectives. *Science of the Total Environment*, **2022**, 838, 156515.
[25] Patel, S., Jamunkar, R., Sinha, D., Patle, T.K., Kant, T., Dewangan, K., Shrivas, K. Recent development in nanomaterials fabricated paper-based colorimetric and fluorescent sensors: A review. *Trends in Environmental Analytical Chemistry*, **2021**, 31, e00136.
[26] Wang, H., Rao, H., Luo, M., Xue, X., Xue, Z., Lu, X. Noble metal nanoparticles growth-based colorimetric strategies: From monocolorimetric to multicolorimetric sensors. *Coordination Chemistry Reviews*, **2019**, 398, 113003.
[27] Sicard, C., Glen, C., Aubie, B., Wallace, D., Jahanshahi-Anbuhi, S., Pennings, K., Daigger, G.T., Pelton, R., Brennan, J.D., Filipe, C.D. Tools for water quality monitoring and mapping using paper-based sensors and cell phones. *Water Research*, **2015**, 70, 360-369.
[28] Durresi, M., Subashi, A., Durresi, A., Barolli, L., Uchida, K. Secure communication architecture for internet of things using smartphones and multi-access edge computing in environment monitoring. *Journal of Ambient Intelligence and Humanized Computing*, **2019**, 10(4), 1631-1640.
[29] Xue, J., Mao, K., Cao, H., Feng, R., Chen, Z., Du, W., Zhang, H. Portable sensors equipped with smartphones for organophosphorus pesticides detection. *Food Chemistry*, **2024**, 434, 137456.
[30] Upadhyay, S., Kumar, A., Srivastava, M., Srivastava, A., Dwivedi, A., Singh, R.K., Srivastava, S. Recent advancements of smartphone-based sensing technology for diagnosis, food safety analysis, and environmental monitoring. *Talanta*, **2024**, 275, 126080.
[31] Hilaluddin, F., Ong, K.K., Norrrahim, M.N.F., Jamari, N.L.-A., Jamal, S.H., Mohd Noor, S.A., Mohd Kasim, N.A., Wan Yunus, W.M.Z., Abdullah, N., Osman, M.J. Recent applications of molecularly imprinted polymer sensors equipped with smartphones for detection of pesticide residues in environmental samples. *Arab Journal of Basic and Applied Sciences*, **2024**, 31(1), 481-504.
[32] Fan, Y., Li, J., Guo, Y., Xie, L., Zhang, G. Digital image colorimetry on smartphone for chemical analysis: A review. *Measurement*, **2021**, 171, 108829.
[33] Ateia, M., Wei, H., Andreescu, S. Sensors for emerging water contaminants: Overcoming roadblocks to innovation. *Environmental Science & Technology*, **2024**, 58(6), 2636-2651.
[34] Abnous, K., Danesh, N.M., Ramezani, M., Alibolandi, M., Emrani, A.S., Lavaee, P., Taghdisi, S.M. A colorimetric gold nanoparticle aggregation assay for malathion based on target-induced hairpin structure assembly of complementary strands of aptamer. *Microchimica Acta*, **2018**, 185(4), 216.

[35] Ariffin, M. I., Jamari, N.L.A., Abdullah, N., Osman, M.J., Ong, K.K., Wan Yunus, W.M.Z., Zulkifli, N.A., Mohd Noor, S.A., Knight, V.F., Ten, S.T., Norrahim M.N.F., Jamal, S.H., Syed Ahmad, S.M.S. Effects of Volume Ratio of Citrate-Capped Gold Nanoparticles (cit-AuNPs) to Malathion, Concentrations of cit-AuNPs and DNA Aptamer on Malathion Colorimetric Detection. *Defence S & T Technical Bulletin*, **2023,** *16*(2), 156-168.

[36] Murdock, R.C., Shen, L., Griffin, D.K., Kelley-Loughnane, N., Papautsky, I., Hagen, J.A. Optimization of a paper-based elisa for a human performance biomarker. *Analytical Chemistry*, **2013**, 85(23), 11634-11642.

[37] Dheyab, M.A., Aziz, A.A., Moradi Khaniabadi, P., Jameel, M.S., Oladzadabbasabadi, N., Mohammed, S.A., Abdullah, R.S., Mehrdel, B. Monodisperse gold nanoparticles: A review on synthesis and their application in modern medicine. *International Journal of Molecular Sciences*, **2022**, 23(13), 7400.

[38] Tan, G., Onur, M.A. Cellular localization and biological effects of 20nm-gold nanoparticles. *Journal of Biomedical Materials Research Part A*, **2018**, 106(6), 1708-1721.

[39] Sangwan, S., Seth, R. Synthesis, characterization and stability of gold nanoparticles (aunps) in different buffer systems. *Journal of Cluster Science*, **2022**, 33(2), 749-764.

[40] Alba-Molina, D., Santiago, A.R.P., Giner-Casares, J.J., Rodríguez-Castellón, E., Martín-Romero, M.T., Camacho, L., Luque, R., Cano, M. Tailoring the orr and her electrocatalytic performances of gold nanoparticles through metal–ligand interfaces. *Journal of Materials Chemistry A*, **2019**, 7(35), 20425-20434.

[41] Park, J.W., Shumaker-Parry, J.S. Structural study of citrate layers on gold nanoparticles: Role of intermolecular interactions in stabilizing nanoparticles. *Journal of the American Chemical Society*, **2014**, 136(5), 1907-1921.

[42] Saidi, D., Obeidat, M., Alsotari, S., Ibrahim, A.-A., Al-Buqain, R., Wehaibi, S., Alqudah, D.A., Nsairat, H., Alshaer, W., Alkilany, A.M. Formulation optimization of lyophilized aptamer-gold nanoparticles: Maintained colloidal stability and cellular uptake. *Heliyon*, **2024**, 10(10).

[43] Bala, R., Dhingra, S., Kumar, M., Bansal, K., Mittal, S., Sharma, R.K., Wangoo, N. Detection of organophosphorus pesticide–malathion in environmental samples using peptide and aptamer based nanoprobes. *Chemical Engineering Journal*, **2017**, 311, 111-116.

[44] Zhang, Y., Yang, L., Sun, C., Huang, C., Zhu, B., Zhang, Q., Chen, D. Aptamer-based sensor for specific recognition of malathion in fruits and vegetables by surface-enhanced raman spectroscopy and electrochemistry combination. *Analytica Chimica Acta*, **2022**, 1221, 340148.

[45] Feng, J., Shen, Q., Wu, J., Dai, Z., Wang, Y. Naked-eyes detection of shigella flexneri in food samples based on a novel gold nanoparticle-based colorimetric aptasensor. *Food Control*, **2019**, 98, 333-341.

## HOW TO CITE THIS ARTICLE

M.I. Ariffin, N. Abdullah, N.L. Jamari, F. Hilaluddin, K.K. Ong, M.J. Osman, J.I.A. Rashid, S.A.M. Noor, W.M.Z.W. Yunus, V.F. Knight, C.K. Ngan, S.T. Ten, M.N. Norrrahim. An Image Analysis-Assisted Paper-Based Colorimetric Aptasensor for Simple and Rapid Malathion Detection. *Adv. J. Chem. A*, 2026, 9(6), 1179-1191.

**DOI: 10.48309/AJCA.2026.563604.1990**
**URL: https://www.ajchem-a.com/article_239922.html**